Inorganic Chemistry

Communication

pubs.acs.org/IC

MOF-Derived Porous Co_3O_4 Hollow Tetrahedra with Excellent Performance as Anode Materials for Lithium-Ion Batteries

Dan Tian,[†,‡,§,∥] Xian-Long Zhou,[†,#,§,∥] Ying-Hui Zhang,[†,‡] Zhen Zhou,*[,†,#,§] and Xian-He Bu*[,†,‡,§]

[†]School of Materials Science and Engineering, National Institute for Advanced Materials, [‡]Department of Chemistry, TKL of Metal- and Molecule-Based Material Chemistry, [#]Key Laboratory of Advanced Energy Material Chemistry (MOE), Institute of New Energy Material Chemistry, and [§]Collaborative Innovation Center of Chemical Science and Engineering (Tianjin), Nankai University, Tianjin 300071, China

Supporting Information

ABSTRACT: Porous Co_3O_4 hollow tetrahedra were prepared through the thermolysis of metal−organic frameworks and presented reversible capacities of 1196 and 1052 mAh g^{-1} at 50 and 200 mA g^{-1} after 60 charge/discharge cycles, respectively. Such excellent performances stem from the well-defined hollow structure of Co_3O_4 tetrahedra.

In the past decade, Co_3O_4 was considered as an anode candidate for lithium-ion batteries (LIBs) because of its large theoretical capacity and facile preparation.[1] However, the actual performance of Co_3O_4 in LIBs is limited by large volume variation upon change/discharge cycling.[2] A feasible approach to addressing these concerns is to construct Co_3O_4 with different morphologies and composite with electrically conductive materials. However, the introduction of too many conductive materials would sacrifice the specific capacity of Co_3O_4 electrodes;[3] therefore, substantial strategies have been explored to pursue various nanostructures to enhance the general performances. In this scenario, Co_3O_4 with various morphologies including nanotubes,[2] hollow spheres,[4] octahedra,[5] nanoboxes,[6] and nanocages[7] has been prepared and exhibited positive effects on the specific capacity.

Recently, hollow nanostructures have been widely explored because of their outstanding features.[8,9] More importantly, these hollow structures can provide not only more shortened pathways for the diffusion of Li^+ but also more large space to mitigate volume expansion upon cycling, contributing to smaller electrode polarization and faster reaction kinetics.[10−12] Therefore, the preparation of various hollow nanostructures has attracted intensive interest. The general routes to obtain them are usually template-assisted methods. However, the use of various templates undergoes additional difficulties in shape preservation and controllable surface coating,[12] and the removal of templates causes additional problems in energy consumption and product quality. Thus, it is urgent to optimize the template-assisted approach to prepare desired hollow structures. Metal−organic frameworks (MOFs) have widely been used to fabricate porous nanostructured materials as self-sacrificing templates.[13] MOFs have proven to be effective templates to prepare porous carbons[14] and metal oxides.[15] Compared with other templates, MOFs provide some superiority related to their robust morphology and large porosity.[16] In addition, the morphology of MOFs could be preserved in the obtained materials. More importantly, the materials derived from MOFs exhibit ameliorated performances when evaluated as energy materials. For example, nitrogen-doped carbon sheets derived from MOFs showed good performances in LIBs and oxygen reduction reactions.[17,18] Wu et al.[19] and Zhang et al.[20] prepared Co_3O_4 hollow dodecahedra from ZIF-67 and found excellent electrochemical performances in electrodes of LIBs or supercapacitors. However, up to now, the preparation of Co_3O_4 hollow tetrahedra derived from MOFs and the application to LIBs were scarcely reported.

In this work, a double-walled tetrahedral MOF, $[Co_3L_2(TPT)_2{\cdot}xG]_n$ (G = guest molecules),[21] was selected as the precursor to prepare hollow Co_3O_4. As illustrated in Scheme 1, the MOF was heated at 500 °C for 4 h in air and then naturally cooled to 25 °C to obtain Co_3O_4 powder. The resulting Co_3O_4 inherited the tetrahedral morphology of the MOF, while the hollow structure was attributed to the thermal treatment of organic parts in the MOF. This approach is simple, tunable, and scalable. The as-prepared Co_3O_4 displayed excellent electrochemical performances as LIB anodes because of their hollow structure.

Scheme 1. Formation of Co_3O_4 Hollow Tetrahedra

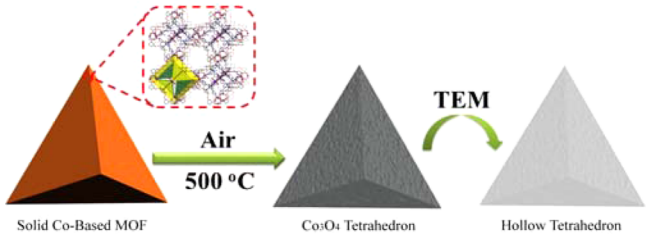

The morphology evolution during the preparation of Co_3O_4 was investigated mainly through field-emission scanning electron microscopy (FESEM), together with transmission electron microscopy (TEM). The crystalline nature of the MOFs was checked with X-ray diffraction (XRD) patterns (Figure S1). Figure 1a shows typical well-defined tetrahedra for the MOFs with sizes of 10−20 μm. Note that both tetrahedra are hierarchical structure. A single tetrahedral structure with smooth

Received: March 9, 2015
Published: August 11, 2015

DOI: 10.1021/acs.inorgchem.5b00544
Inorg. Chem. 2015, 54, 8159−8161

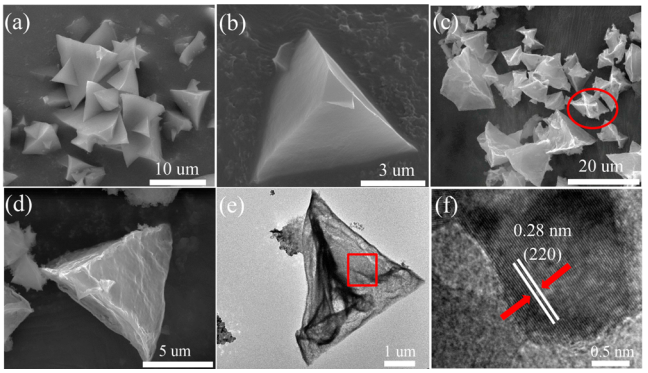

Figure 1. FESEM images for MOFs (a and b) and Co_3O_4 (c and d) and TEM (e) and HRTEM images (f) for Co_3O_4.

surface is further observed by a magnified FESEM image (Figure 1b), and its solid structure is identified by TEM (Figure S2).

Interestingly, configurations similar to those of the MOFs and some twin tetrahedral structures were perfectly maintained in the calcined products (Figure 1c) but with rough surfaces in comparison with the precursor (Figure 1d). The rough surface of Co_3O_4 should be attributed to the massive loss of inner organic contents, which is supported by its hollow framework revealed in the TEM image (Figure 1e). In addition, the high-resolution TEM (HRTEM) image (Figure 1f), taken over the area in Figure 1e, displays lattice fringes of well-crystallized Co_3O_4, with a spacing of 2.8 Å corresponding to the (220) interplane of Co_3O_4 with a curb structure.

The crystallographic structure of calcined powders was checked with the XRD patterns in Figure S3a; the peaks well match the cubic Co_3O_4 (JPCDS 42-1467), which suggests complete transition of MOFs to Co_3O_4. X-ray photoelectron spectroscopy (XPS) was conducted (Figure S4) to further determine the chemical composition and valence of the product. The IV-type curves (Figure S3b) indicate the presence of micropores inherited from porous MOF precursors. Fitting of the N_2 isotherm of Co_3O_4 materials shows the Brunauer–Emmett–Teller (BET) surface area as 32 $m^2\ g^{-1}$. Notably, the pores in Co_3O_4 range mostly between 17 and 30 nm. The ingenious structure renders Co_3O_4 some superiority for lithium storage and diffusion, as well as enough space to accommodate large volume variation during cycling.

The electrochemical performances of tetrahedral Co_3O_4 were investigated in half-cells. Figure 2a displays the cyclic voltammetry (CV) cycles under a sweeping rate of 0.1 mV s^{-1} in the range of 0.01–3.00 V. Obviously, the first cycle varies from the following ones. The peak at 0.82 V, only in the first cycle, is related to solid electrolyte interface (SEI) films. From the second cycle, there are a pair of redox peaks at 1.07 and 2.08 V, which are

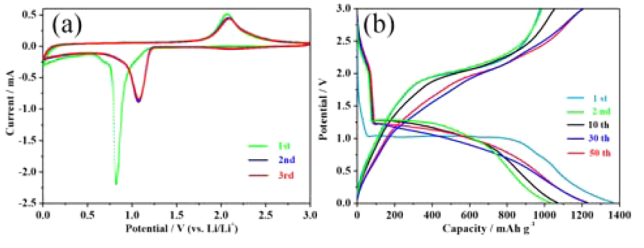

Figure 2. (a) Initial three-cycle CV curves and (b) galvanostatic charge/discharge curves of Co_3O_4.

associated with the reaction from Co_3O_4 to cobalt accompanied by the appearance of Li_2O, and the corresponding reverse reaction. Obviously, the curves almost overlap after the first cycle, demonstrating that Co_3O_4 electrodes were somewhat stable.

The cycling stability was further tested at 50 mA g^{-1}, and the results are shown in Figure 2b for various cycles. The discharge and charge capacities are 1370.0 and 975.8 mA h g^{-1}, respectively, with a Coulombic efficiency (CE) of 71.6% in the first cycle. Such a low CE stems from the formation of SEI films.[7] The discharge platform at ~1.0 V is ascribed to the conversion of Co_3O_4 to Co^0 and the formation of Li_2O, which disappears in the following cycles.[22] However, in the subsequent cycle, the charge and discharge capacities are 985 and 1034 mA h g^{-1}, respectively, and CE is remarkably increased to 95.3%. The capacity of Co_3O_4 remained 1196 mAh g^{-1} after 60 cycles (Figure 3a), which is

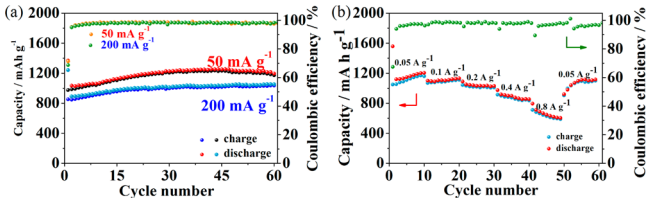

Figure 3. (a) Cyclic and (b) rate performances of Co_3O_4 electrodes.

greater than the theoretical value of Co_3O_4, and the CE of the Co_3O_4 electrode reached nearly 98%. Impressively, with the cycle going on, the capacity increases slightly. The phenomena of gradually increasing the capability and extra capacity have also been reported on other transition-metal oxides[23,24] and were interpreted in terms of the reversible reactions of some composition in SEI films or the gradual electrode activation.[25,26]

Moreover, the porous Co_3O_4 electrode still exhibits a robust performance at 200 mA g^{-1}, with 1052 mAh g^{-1} after 60 cycles (Figure 3a). The reversible capacity of hollow Co_3O_4 tetrahedra is much higher than those of most previous reports on MOF-derived Co_3O_4 samples (Table S1).[19,22,S1–S5] Note that the CE of the porous Co_3O_4 electrode reaches nearly 98% after the second cycle, indicative of the high reversibility of the conversion reaction between Li and Co_3O_4.

Fast discharge/charge capability is another key aspect for LIBs; hence, the rate performance of Co_3O_4 electrodes was checked from charge/discharge cycles under different current densities (Figure 3b). The electrode delivered high reversible capacities of 1190 mA h g^{-1} at 50 mA g^{-1}, 1125 mA h g^{-1} at 100 mA g^{-1}, 1035 mA h g^{-1} at 200 mA g^{-1}, and 875 mA h g^{-1} at 400 mA g^{-1}. When the current density increased to 0.8 A g^{-1}, the corresponding capacity maintained as 606 mA h g^{-1}, demonstrating excellent rate capability. More importantly, the capacity could recover to 1125 mA h g^{-1} while the current density returned to 50 mA g^{-1}.

To further investigate the reason why the Co_3O_4 electrode displayed gradually increasing capacity during cycling, we performed electrochemical impedance spectroscopy (EIS). The Nyquist plots in Figure S5a show a depressed semicircle in the high-frequency region and a sloping line at the low-frequency region. The semicircle corresponds to the electrode/electrolyte interfacial resistance; the sloping line is attributed to Warburg impedance, which is related to Li^+ diffusion into the electrode/electrolyte interface. According to the equivalent circuit (Figure S5b), Rs denotes the electrolyte resistance, R1 and CPE1 represent the resistance and constant phase element (CPE) of the SEI films, respectively, R2 and CPE2 are the

DOI: 10.1021/acs.inorgchem.5b00544
Inorg. Chem. 2015, 54, 8159–8161

charge-transfer resistance and CPE of the electrode/electrolyte interface, respectively, and W1 denotes the Warburg impedance.[27,28] Notably, the fitted results on the basis of Figure S5b agree well with the experimental values for both the 1st and 20th cycles in Figure S5a. The values of Rs, R1, and R2 for the 1st cycle are 6.4, 44.6, and 1080.0 Ω, respectively. The corresponding values for the 20th cycle are 0.9, 58.0, and 586.0 Ω, respectively. Although R1 increased, because of the formation of new SEI films, the lower R2 demonstrated smaller charge-transfer resistance of the electrode/electrolyte interface. This indicates that the ion diffusion and electron transfer of the 20th cycle are much faster than those of the first one in the charge/discharge cycles and thus lead to the gradually increasing capacity of Co_3O_4.[29] Moreover, the TEM image of the Co_3O_4 electrode cycled 20 times at 200 mA g^{-1} was collected to check the structural stability of Co_3O_4. Obviously, the structure of the hollow tetrahedron was still maintained even after repeated fast charge and discharge cycles, although the surface became rougher (Figure S5c) because of the appearance of SEI films and amorphous Li_2O.[30] Hence, the large lithium-storage capacity and excellent rate performance are probably ascribed to the special structure.

In summary, porous Co_3O_4 hollow tetrahedra were prepared with MOFs as self-sacrificing templates. Profiting from the highly porous hollow structure, the obtained material exhibited a large lithium-storage capacity, superior rate performance, and cyclic stability as an anode material for LIBs. These results manifest that tetrahedral Co_3O_4 derived from MOFs is a promising candidate as a next-generation LIB anode material.

■ ASSOCIATED CONTENT

Supporting Information

The Supporting Information is available free of charge on the ACS Publications website at DOI: 10.1021/acs.inorgchem.5b00544.

Detailed experimental procedures; XRD patterns, a TGA curve, and a TEM image of MOFs; XPS of Co_3O_4; and a comparison table of our sample and previously reported Co_3O_4 anode materials derived from MOFs (PDF)

■ AUTHOR INFORMATION

Corresponding Authors

*E-mail: zhouzhen@nankai.edu.cn.
*E-mail: buxh@nankai.edu.cn.

Author Contributions

‖D.T. and X.-L.Z. contributed equally to this work.

Notes

The authors declare no competing financial interest.

■ ACKNOWLEDGMENTS

This work was supported by the MOE Innovation Team (Grant IRT13022) and the NSFC (Grant 21421001) in China.

■ REFERENCES

(1) Reddy, M. V.; Subba Rao, G. V.; Chowdari, B. V. *Chem. Rev.* **2013**, *113*, 5364−5457.
(2) Lou, X. W.; Deng, D.; Lee, J. Y.; Feng, J.; Archer, L. A. *Adv. Mater.* **2008**, *20*, 258−262.
(3) Hu, L.; Yan, N.; Chen, Q. W.; Zhang, P.; Zhong, H.; Zheng, X. R.; Li, Y.; Hu, X. Y. *Chem. - Eur. J.* **2012**, *18*, 8971−8977.
(4) Xia, X. H.; Tu, J. P.; Wang, X. L.; Gu, C. D.; Zhao, X. B. *Chem. Commun.* **2011**, *47*, 5786−5788.
(5) Xiao, X. L.; Liu, X. F.; Zhao, H.; Chen, D.; Liu, F.; Xiang, J.; Hu, Z.; Li, Y. *Adv. Mater.* **2012**, *24*, 5762−5766.
(6) He, T.; Chen, D. R.; Jiao, X. L.; Wang, Y. L. *Adv. Mater.* **2006**, *18*, 1078−1082.
(7) Liu, D. Q.; Wang, X.; Wang, X. B.; Tian, W.; Bando, Y.; Golberg, D. *Sci. Rep.* **2013**, *3*, 2543.
(8) Wu, R. B.; Qian, X. K.; Zhou, K.; Wei, J.; Lou, J.; Ajayan, P. M. *ACS Nano* **2014**, *8*, 6297−6303.
(9) Geng, H. B.; Ming, H.; Ge, D. H.; Zheng, J. W.; Gu, H. W. *Electrochim. Acta* **2015**, *157*, 1−7.
(10) Hu, J.; Chen, M.; Fang, X. S.; Wu, L. M. *Chem. Soc. Rev.* **2011**, *40*, 5472−5491.
(11) Li, Y. S.; Shi, J. L. *Adv. Mater.* **2014**, *26*, 3176−3205.
(12) Wang, Z.; Zhou, L.; Lou, X. W. *Adv. Mater.* **2012**, *24*, 1903−1911.
(13) Zou, F.; Hu, X.; Li, Z.; Qie, L.; Hu, C.; Zeng, R.; Jiang, Y.; Huang, Y. *Adv. Mater.* **2014**, *26*, 6622−6628.
(14) Liu, B.; Shioyama, H.; Akita, T.; Xu, Q. *J. Am. Chem. Soc.* **2008**, *130*, 5390−5391.
(15) Cho, W.; Lee, Y. H.; Lee, H. J.; Oh, M. *Adv. Mater.* **2011**, *23*, 1720−1723.
(16) Zhang, L.; Wu, H.; Xu, R.; Lou, X. W. *CrystEngComm* **2013**, *15*, 9332−9335.
(17) Zheng, F.; Yang, Y.; Chen, Q. *Nat. Commun.* **2014**, *5*, 5261−5270.
(18) Zhong, H.; Wang, J.; Zhang, Y.; Xu, W.; Xing, W.; Xu, D.; Zhang, Y.; Zhang, X. *Angew. Chem., Int. Ed.* **2014**, *53*, 14235−14239.
(19) Wu, R.; Qian, X.; Rui, X.; Liu, H.; Yadian, B. L.; Zhou, K.; Wei, J.; Yan, Q.; Feng, X.; Long, Y.; Wang, L.; Huang, Y. *Small* **2014**, *10*, 1932−1938.
(20) Zhang, Y.; Wang, Y.; Xie, Y.; Cheng, T.; Lai, W.; Pang, H.; Huang, W. *Nanoscale* **2014**, *6*, 14354−14359.
(21) Tian, D.; Chen, Q.; Li, Y.; Zhang, Y. H.; Chang, Z.; Bu, X. H. *Angew. Chem., Int. Ed.* **2014**, *53*, 837−841.
(22) Ge, D.; Geng, H.; Wang, J.; Zheng, J.; Pan, Y.; Cao, X.; Gu, H. *Nanoscale* **2014**, *6*, 9689−9694.
(23) Wang, R.; Xu, C.; Sun, J.; Gao, L. *Sci. Rep.* **2014**, *4*, 7171.
(24) Li, D.; Ding, L.; Wang, S.; Cai, D.; Wang, H. *J. Mater. Chem. A* **2014**, *2*, 5625−5630.
(25) Xu, X.; Cao, R.; Jeong, S.; Cho, J. *Nano Lett.* **2012**, *12*, 4988−4991.
(26) Bresser, D.; Paillard, E.; Kloepsch, R.; Krueger, S.; Fiedler, M.; Schmitz, R.; Baither, D.; Winter, M.; Passerini, S. *Adv. Energy Mater.* **2013**, *3*, 513−523.
(27) Shen, W.; Wang, C.; Xu, Q.; Liu, H.; Wang, Y. *Adv. Energy Mater.* **2015**, *5*, 10.1002/aenm.201400982.
(28) Luo, Y.; Zhou, X.; Zhong, Y.; Yang, M.; Wei, J.; Zhou, Z. *Electrochim. Acta* **2015**, *154*, 136−141.
(29) Zhong, Y.; Yang, M.; Zhou, X.; Luo, Y.; Wei, J.; Zhou, Z. *Adv. Mater.* **2015**, *27*, 806−812.
(30) Zhou, X. L.; Zhong, Y. R.; Yang, M.; Zhang, Q.; Wei, J. P.; Zhou, Z. *ACS Appl. Mater. Interfaces* **2015**, *7*, 12022−12029.

DOI: 10.1021/acs.inorgchem.5b00544
Inorg. Chem. 2015, 54, 8159−8161